ISSN (Print) 1226-1750
ISSN (Online) 2233-6656
Journal of Magnetics 21(2), 164-167 (2016) http://dx.doi.org/10.4283/JMAG.2016.21.2.164

Effect of Boron Additions on Glass Formation and Magnetic Properties of Fe-Co-Ti-Zr-B Amorphous Ribbons

Sumin Kim, Bo Kyeong Han, and Haein Choi-Yim*

Department of Physics, Sookmyung Women's University, Seoul 04310, Republic of Korea

(Received 2 May 2016, Received in final form 12 May 2016, Accepted 12 May 2016)

The effect of the B additions on glass formation and magnetic properties is reported for the $Fe_{(87-x-y)}Co_yTi_7Zr_6B_x$ (x = 2, 4, 6 and y = 35, 40) alloy system. The ribbon samples with the width of 2 mm for each composition were prepared by the melt spinning technique; furthermore, their phase information was obtained from X-ray diffraction. Glass formation and magnetic properties were measured using differential scanning calorimetry and vibrating sample magnetometer respectively. The $Fe_{45}Co_{40}Ti_7Zr_6B_2$ (x = 2 and y = 40) system has the nanocrystalline phase identified as α-Fe, as well as the amorphous phase, whereas all other alloys are fully amorphous. It is associated with the role of B on the glass formation. The widest supercooled liquid region is obtained as 71 K at x = 4 (both y = 35 and 40). The saturation magnetization decreases with the increase of the amount of the B addition, and the highest value is 1.59 T as x = 2 and y = 35 for this alloy system.

Keywords : Fe-based, amorphous, ribbon, boron addition

1. Introduction

Fe-based ferromagnetic metallic glasses are of current interest in engineering due to their excellent soft magnetic properties including high saturation magnetization (M_s) and permeability as well as low core loss and coercivity. In addition, Fe-based soft magnetic amorphous materials have low material cost, ultrahigh strength and high corrosion resistance [1-7]. Nevertheless, Fe-based amorphous alloys can hardly replace the traditional Si electrical steels which have no dimensional limit due to the limited glass forming ability (GFA) of amorphous alloys. In order to improve their GFA, Fe-based amorphous alloys have involved various glass forming metallic elements, such as Cu, Nb, Zr, Mo and Ta, and they usually replace Fe concentration [8, 9]. However, non-ferromagnetic metallic elements cause a decrease in M_s and also lead to the increase of the price of the material. Therefore, it is necessary to develop novel Fe-based metallic glasses with both high GFA and M_s.

In general, it is well known that the contents of metalloid elements, such as P, C, Si, and B, play a significant role in the formation of metallic glasses in the Fe-based amorphous alloys [10-13]. In particular, due to atomic interaction and large atomic size differences between B and transition metals, the suitable ratios of B to transition metals, such as Fe, Co, and Ni, lead to the enhancement of its GFA and thermal stability of amorphous alloys. In addition, the proportion of B to transition metals affects their magnetic properties. However, the addition of metalloid elements usually makes the Fe-based amorphous alloys more brittle. Therefore, in order to overcome industrial limitations, further research is needed on the effects of the B content in a wide range on glass formations and various properties of Fe-based amorphous alloys.

In a previous study, we reported the soft magnetic and mechanical properties of $Fe_{(87-x-y)}Co_yTi_7Zr_6B_x$ (x = 2, 4 and y = 20, 25, 30, 35, 40) alloys [14, 15]. Yet, further research on the GFA of these alloys is necessary. The supercooled liquid region (ΔT_x) defined as the temperature interval between the glass transition temperature (T_g) and crystallization temperature (T_x) is the index for the GFA. Based on our previous research, in the present study, we focused on the effects of minor B additions on glass forming and magnetic properties for $Fe_{(87-x-y)}Co_yTi_7Zr_6B_x$ (x = 2, 4, 6 and y = 35, 40). Fe was replaced by B. Our goal was not to obtain the best value of properties such as ΔT_x and M_s, but to inspect the effect of the B content on the glass forming and magnetic properties of the Fe-based amorphous alloy.

*Corresponding author: Tel: +82-2-710-9239
Fax: +82-2-710-9239, e-mail: haein@sm.ac.kr

2. Experimental Details

Alloys with the composition of $Fe_{(87-x-y)}Co_yTi_7Zr_6B_x$ (x = 2, 4, 6 and y = 35, 40) were studied. High purity Fe (99.95%), Co (99.95%), Ti (99.995%), Zr (99.8%) and B (99.5%) were used to obtain ingots with the masses of 6 g for each composition by arc-melting under a Ti-gettered Ar atmosphere. To maximize compositional homogeneity, all ingots were re-melted four times. From the master alloy ingots, the ribbons 2 mm in width and 20-30 μm in thickness were prepared using the melt spinning under Ar atmosphere at a roll speed of 56.3 m/s. The structure of the obtained Fe-based ribbons was examined using X-ray diffraction (XRD) with Cu-Kα radiation. A pyrolytic graphite diffracted-beam monochromator was used to minimize the fluorescence background caused by Cu-Kα source on Fe target. The grain size of Fe was calculated by broadening of the XRD patterns using Scherrer equation [16], $D = K\lambda/\beta\cos\theta$, where D is crystallite size, K is a shape factor of the average crystallite, λ is wavelength of incident radiation, and β is full width at half maximum. Thermal stability associated with the glass transition temperature (T_g), crystallization temperature (T_x) and supercooled liquid region ($\Delta T_x = T_x - T_g$) was investigated by differential scanning calorimetry (DSC) and thermo-mechanical analysis (TMA) under a flowing Ar atmosphere and constant heating up to 1073 K at the heating rate of 0.34 K/s. T_g was determined by TMA from the inter-section of two tangential lines in the dimensional change versus temperature profiles. The saturation magnetization (M_s) at room temperature was measured using a vibrating sample magnetometer (VSM) under in-plane applied magnetic field ranging from −800 kA/m-800 kA/m.

3. Results and Discussion

Figure 1 shows the XRD patterns of all the melt-spun $Fe_{(87-x-y)}Co_yTi_7Zr_6B_x$ (x = 2, 4, 6 and y = 35, 40) alloys. Only broad halo hump without a crystalline peak can be seen for most these ribbon samples, indicating the formation of a glassy phase. However, the $Fe_{45}Co_{40}Ti_7Zr_6B_2$ (x = 2 and y = 40) shows a unique pattern. The crystalline peaks identified as α-Fe (ferrite) coexist with the amorphous phase. In the typical Fe-based amorphous alloys, the crystallization temperature is higher than the Curie temperature (T_c) of the amorphous phase. Consequently, the ferromagnetic α-Fe from the amorphous matrix is precipitated via the crystallization process above T_c [17, 18]. According to the Scherrer equation, the calculated mean grain size for the α-Fe phase is about 39 nm. The crystalline peaks disappear with the additions of B in

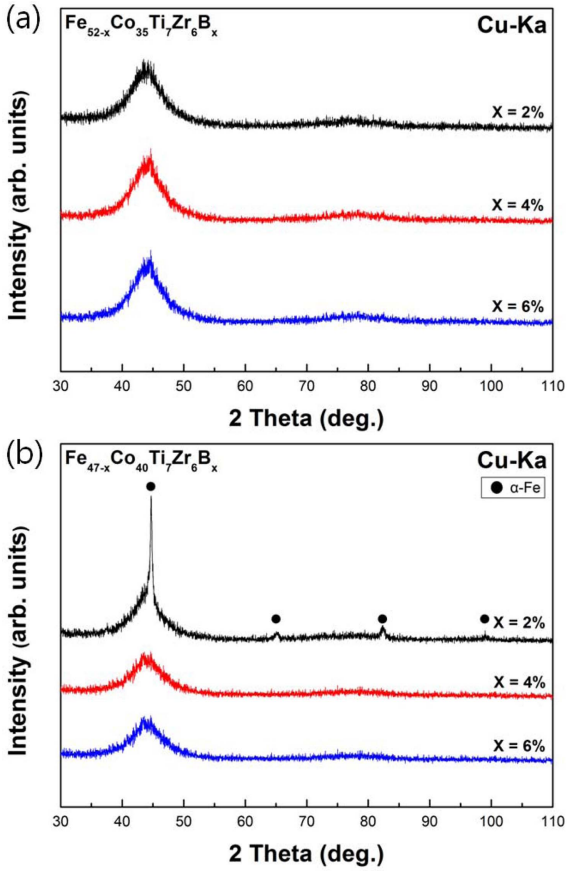

Fig. 1. (Color online) The XRD patterns of (a) $Fe_{(52-x)}Co_{35}Ti_7Zr_6B_x$ (x = 2, 4, 6 at.%) as-spun ribbons and (b) $Fe_{(47-x)}Co_{40}Ti_7Zr_6B_x$ (x = 2, 4, 6 at.%) as-spun ribbons.

$Fe_{(47-x)}Co_{40}Ti_7Zr_6B_x$ (x = 2, 4, 6) alloys. It can be observed that the additions of B play an important role in glass formation.

Figure 2 shows the DSC curves of $Fe_{(87-x-y)}Co_yTi_7Zr_6B_x$ (x = 2, 4, 6 and y = 35, 40) alloys. T_g and T_x are marked by arrows in Figure 2. T_g did not appear for any of the DSC tested alloy, so the TMA testing was conducted to obtain specific values of T_g in this study. ΔT_x is the temperature difference measured during heating between the T_x and T_g. Therefore, ΔT_x is usually used to characterize thermal stability of an amorphous alloy. In particular, it is a criterion of the glass formation ability (GFA) in Fe-based amorphous alloys [19-21]. $Fe_{(52-x)}Co_{35}Ti_7Zr_6B_x$ (x = 2, 4, 6) and $Fe_{(47-x)}Co_{40}Ti_7Zr_6B_x$ (x = 2, 4, 6) ribbons have the values of ΔT_x in the range of 4-71 K and 3-29 K respectively. Based on these results, the largest values of ΔT_x were obtained as the B content of 4 at.%. In the B content of 6 at.%, the values of T_g and T_x are very similar, so ΔT_x is much smaller than the others. These two statements indicate that the critical B content for thermal stability can exist between the B content of 2 and 6 at.%.

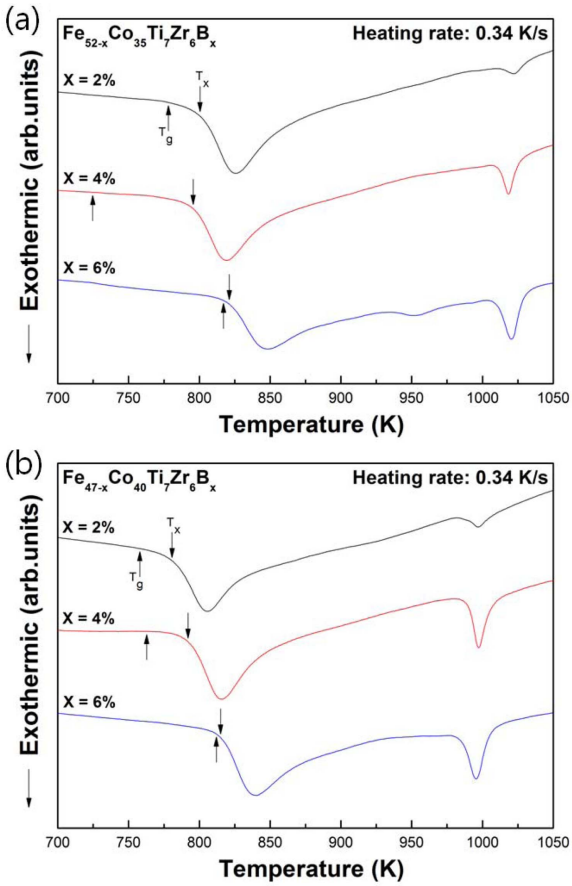

Fig. 2. (Color online) The DSC curves of (a) $Fe_{(52-x)}Co_{35}Ti_7Zr_6B_x$ (x = 2, 4, 6 at.%) as-spun ribbons and (b) $Fe_{(47-x)}Co_{40}Ti_7Zr_6B_x$ (x = 2, 4, 6 at.%) as-spun ribbons.

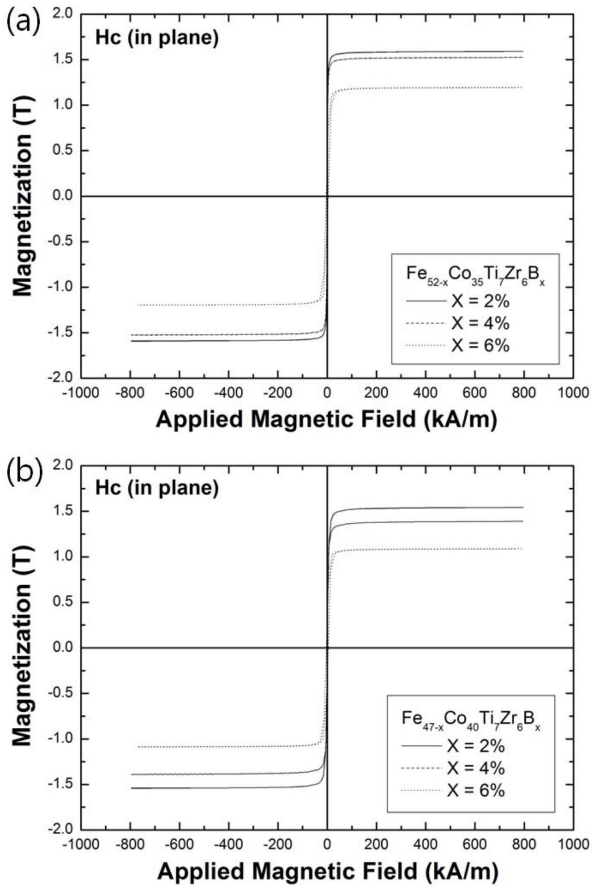

Fig. 3. Hysteresis loops of (a) $Fe_{(52-x)}Co_{35}Ti_7Zr_6B_x$ (x = 2, 4, 6 at.%) as-spun ribbons and (b) $Fe_{(47-x)}Co_{40}Ti_7Zr_6B_x$ (x = 2, 4, 6 at.%) as-spun ribbons.

In this study, $Fe_{48}Co_{35}Ti_7Zr_6B_4$ (x = 4 and y = 35) has the widest ΔT_x of 71 K among $Fe_{(87-x-y)}Co_yTi_7Zr_6B_x$ (x = 2, 4, 6 and y = 35, 40) as-spun ribbons. The characteristic temperatures of T_g, T_x and ΔT_x deduced from Figure 2 are specified in Table 1. Also, the variation of ΔT_x as content of B is illustrated in Figure 4 (a).

The M_s of the $Fe_{(87-x-y)}Co_yTi_7Zr_6B_x$ (x = 2, 4, 6 and y = 35, 40) alloys were obtained according to the measured hysteresis M-H loops at room temperature as shown in Figure 3. All loops exhibit typical soft magnetic behaviors. The dependence of M_s on the B content is depicted in Figure 4 (b). With the increasing atomic percentage of B from 2 to 6 at.%, the M_s gradually decreases from 1.59 T to 1.20 T for the $Fe_{(52-x)}Co_{35}Ti_7Zr_6B_x$ (x = 2, 4, 6) alloy system and from 1.54 T to 1.09 T for the $Fe_{(47-x)}Co_{40}Ti_7Zr_6B_x$ (x = 2, 4, 6) alloy system. $Fe_{50}Co_{35}Ti_7Zr_6B_2$ (x = 2 and y = 35) has the highest M_s of 1.59 T among $Fe_{(87-x-y)}Co_yTi_7Zr_6B_x$ (x = 2, 4, 6 and y = 35, 40) alloy system. The decrease in M_s can be explained by the decrease of Fe content. The values of M_s are summarized in Table 1.

Table 1. Thermal and magnetic properties of $Fe_{(87-x-y)}Co_yTi_7Zr_6B_x$ (x = 2, 4, 6 at.%, and y = 35, 40 at.%) as-spun ribbons.

Alloys	Thermal Properties			Magnetic Properties	
	T_g (K)	T_x (K)	ΔT_x (K)	M_s (emu/g)	M_s (T)
$Fe_{50}Co_{35}Ti_7Zr_6B_2$	778	800	22	166.1	1.59
$Fe_{48}Co_{35}Ti_7Zr_6B_4$	724	795	71	160.6	1.53
$Fe_{46}Co_{35}Ti_7Zr_6B_6$	817	821	4	127.0	1.20
$Fe_{45}Co_{40}Ti_7Zr_6B_2$	758	780	22	160.1	1.54
$Fe_{43}Co_{40}Ti_7Zr_6B_4$	763	792	29	145.6	1.39
$Fe_{41}Co_{40}Ti_7Zr_6B_6$	812	815	3	114.9	1.09

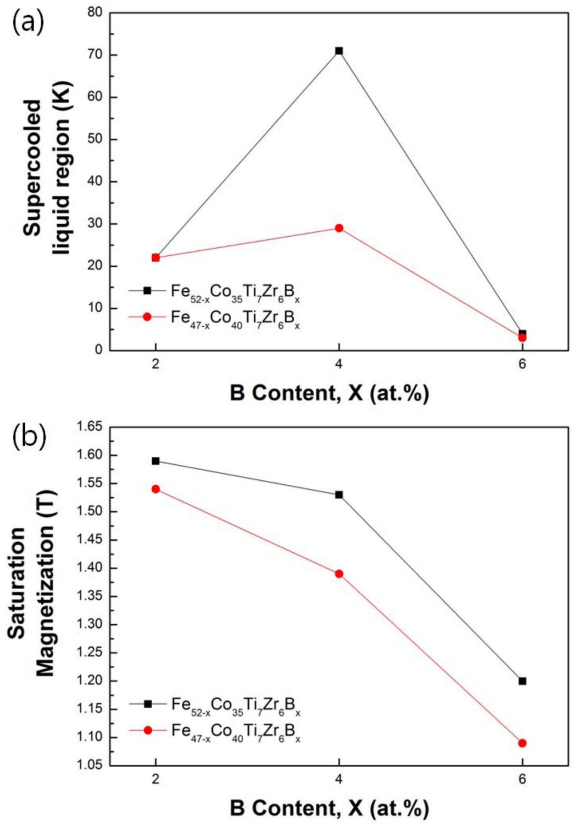

Fig. 4. (Color online) Variation of (a) supercooled liquid region and (b) saturation magnetization as the content of B of $Fe_{(87-x-y)}Co_yTi_7Zr_6B_x$ (x = 2, 4, 6 at.%, and y = 35, 40 at.%) as-spun ribbons.

4. Conclusion

The present study investigated the effect of the B additions on glass formation and magnetic properties for $Fe_{(87-x-y)}Co_yTi_7Zr_6B_x$ (x = 2, 4, 6 and y = 35, 40) system. The ribbon of $Fe_{45}Co_{40}Ti_7Zr_6B_2$ (x = 2 and y = 40) showed crystalline peaks as α-Fe, as well as the amorphous phase hump in the XRD patterns. Other alloys were identified as fully amorphous. The DSC and TMA curves provide the GFA of $Fe_{(87-x-y)}Co_yTi_7Zr_6B_x$ (x = 2, 4, 6 and y = 35, 40) alloys. The widest ΔT_x was obtained as the B content of 4 at.% (both y = 35 and 40). This finding implies the existence of the critical B content for ΔT_x. We found that the largest value of the ΔT_x was 71 K as x = 4 and y = 35. Through the M-H curves, we demonstrated that the addition of B contributes to the decrease of the values of M_s due to the decrease of Fe content. We also found that the highest value of M_s was 1.59 T as x = 2 and y = 35 for this specific system.

The tendencies of ΔT_x and M_s as a function of the B content were confirmed in the present study. However, the full scale of the B contents was not investigated. Detailed measurements about the effect of B on glass formation and magnetic properties are currently in progress.

Acknowledgment

This research was supported by Basic Science Research Program through the National Research Foundation of Korea (NRF) funded by the Ministry of Science, ICT & Future Planning (2015005294).

References

[1] P. Duwez and S. C. H. Lin, J. Appl. Phys. **38**, 4096 (1967).
[2] J. Durand, IEEE Trans. Magn. **12**, 945 (1976).
[3] C. Suryanarayana and A. Inoue, Int. Mater. Rev. **58**, 131 (2013).
[4] M. Mitera, T. Masumoto, and N. S. Kazama, J. Appl. Phys. **50**, 7609 (1979).
[5] A. Inoue, B. L. Shen, and C. T. Chang, Acta Mater. **52**, 4093 (2004).
[6] B. L. Shen, A. Inoue, and C. T. Chang, Appl. Phys. Lett. **85**, 4911 (2004).
[7] S. J. Pang, T. Zhang, K. Asami, and A. Inoue, Acta Mater. **50**, 489 (2002).
[8] W. H. Wang, Prog. Mater Sci. **52**, 540 (2007).
[9] Z. B. Zhao, H. Li, J. Gao, Y. Wu, and Z. P. Lu, Intermetallics **19**, 1502 (2011).
[10] M. Mitera, M. Naka, T. Masumoto, N. Kazama, and K. Watanabe, Phys. Stat. Sol. (a) **49**, 163 (1978).
[11] A. Makino, T. Kubota, and C. T. Chang, Mater. Trans. JIM **48**, 3024 (2007).
[12] J. H. Zhang, C. T. Chang, A. D. Wang, and B. L. Shen, J. Non-Cryst. Solids **358**, 1443 (2012).
[13] Z. Q. Liu and Z. F. Zhang, J. Appl. Phys. **114**, 243519 (2013).
[14] B. Han, S. Kim, and H. Choi-Yim, J. Nanosci. Nanotechno. **16**, 1 (2016).
[15] S. Kim, B. K. Han, D. T. Quach, D-H. Kim, Y. K. Kim, and H. Choi-Yim, Curr. Appl. Phys. **16**, 515 (2016).
[16] M. P. Klug and L. F. Alexanader, X-ray Diffraction Procedures for Polycrystalline and Amorphous Materials, John Wiley & Sons, New York (1974) pp. 634.
[17] Y. Takahara and N. Narita, Mater. Trans. JIM **41**, 1077 (2000).
[18] R. Onodera, S. Kimura, K. Watanabe, Y. Yokoyama, A. Makino, and K. Koyama, J. Alloy. Compd. **637**, 213 (2015).
[19] A. Inoue, T. Zhang, and T. Masumoto, J. Non.-Cryst. Solids **156-158**, 437 (1993).
[20] T. D. Shen and R. B. Schwarz, Appl. Phys. Lett. **75**, 49 (1999).
[21] B. Yao, Y. Zhang, L. Si, H. Tan, and Y. Li, J. Alloy. Comp. **370**, 1 (2004).